

https://dspace.org/

A computer and experimental simulation of Stirling cycle machines

Berchowitz, David M

2011-10-04
http://hdl.handle.net/10539/10477

Downloaded from a DSpace repository. https://dspace.org/

TEST 8.

PLOT ERROR ±5.0WATTS

FREQUENCY 4.350HZ

CHARGE PRESSURE 0.703 BARS

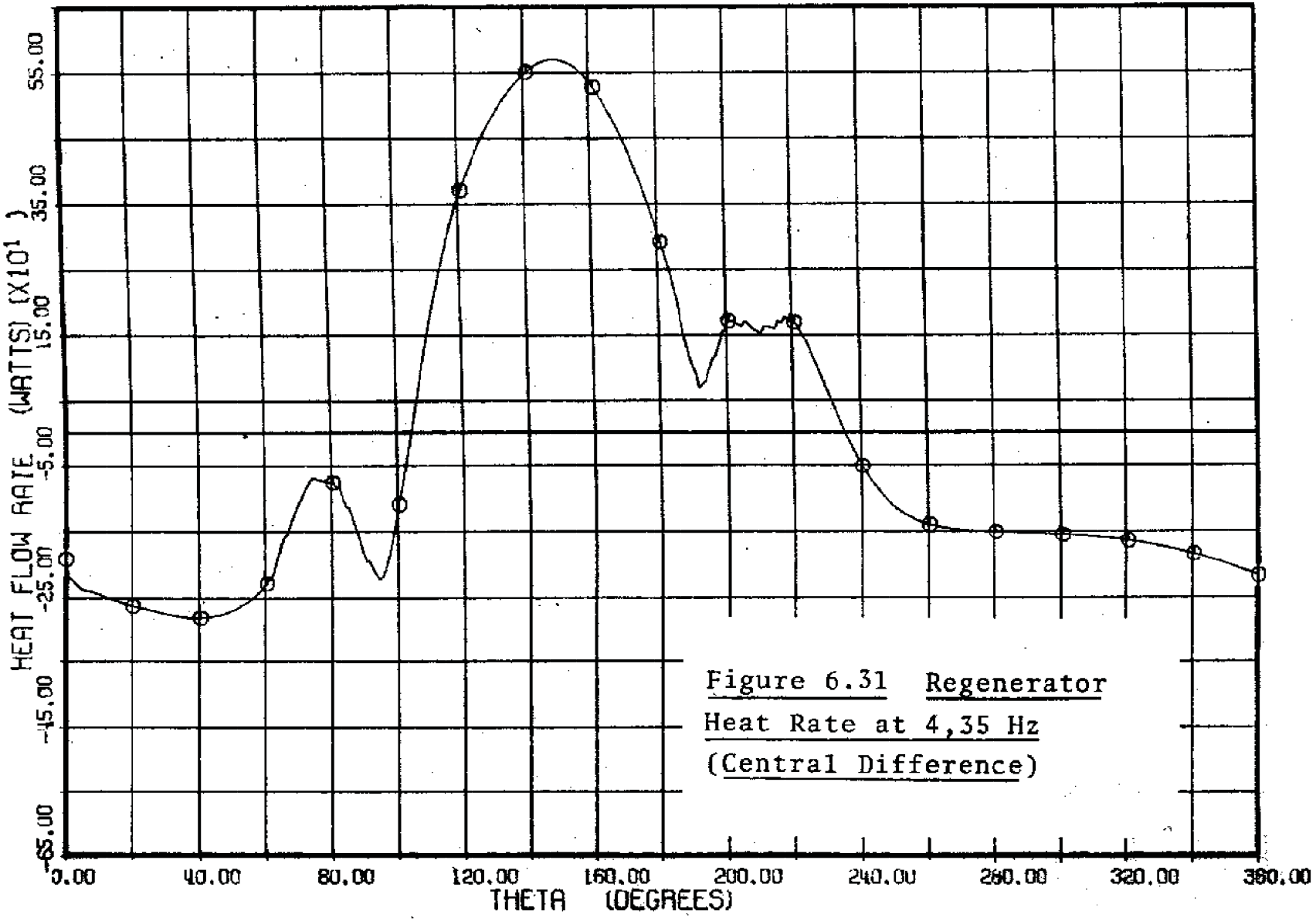


Figure 6.31 Regenerator Heat Rate at 4,35 Hz (Central Difference)

TEST 8.

FREQUENCY 4.350HZ

CHARGE PRESSURE 0.703 BARS

PLOT ERROR ±0.5K

SIMULATION AVG COMPR TEMP ⊙	225.484K
EXPERIMENTAL AVG COMPR TEMP	241.400K
SIMULATION AVG EXPAN TEMP △	304.781K
EXPERIMENTAL AVG EXPAN TEMP	341.700K

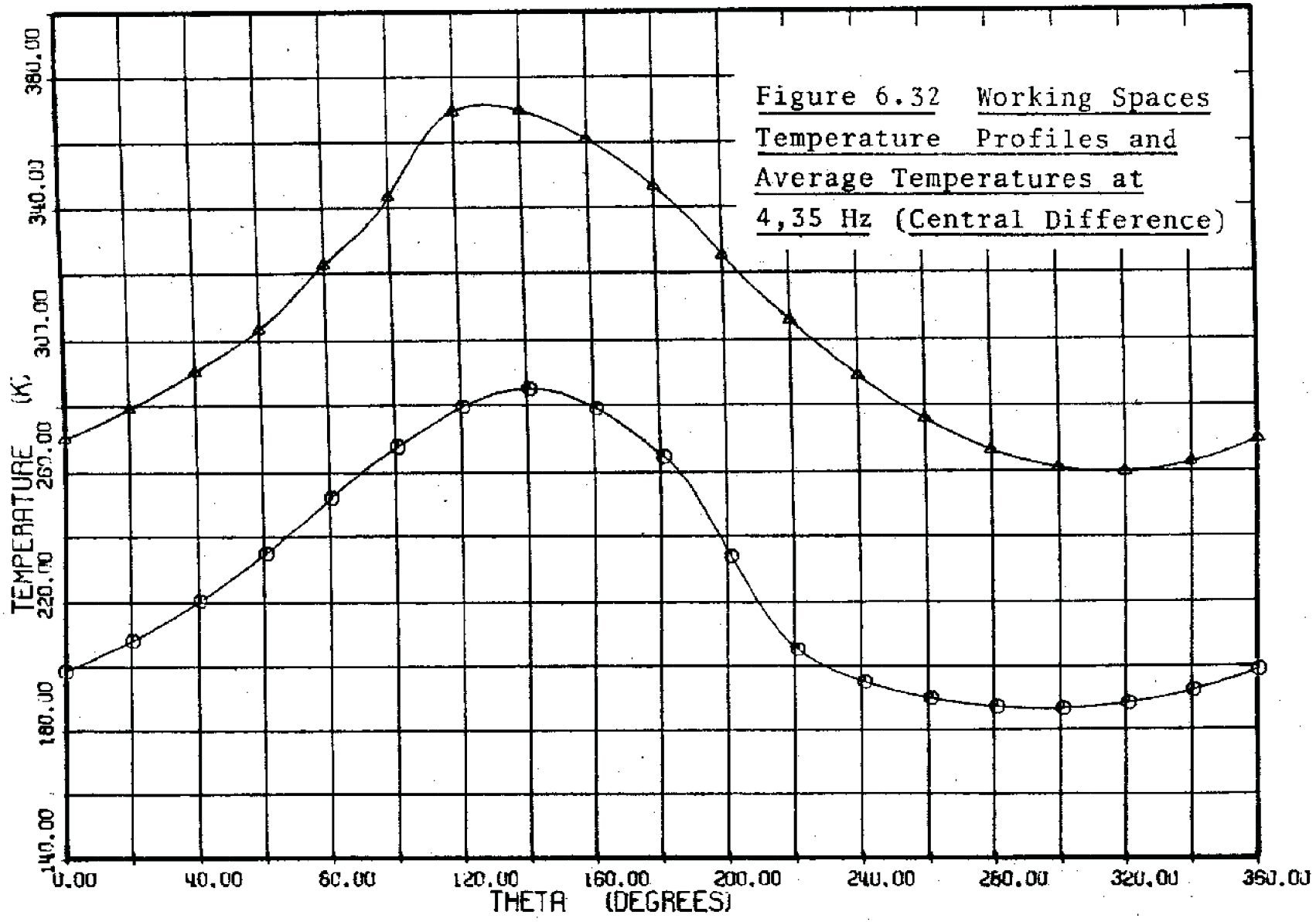


Figure 6.32 Working Spaces Temperature Profiles and Average Temperatures at 4,35 Hz (Central Difference)

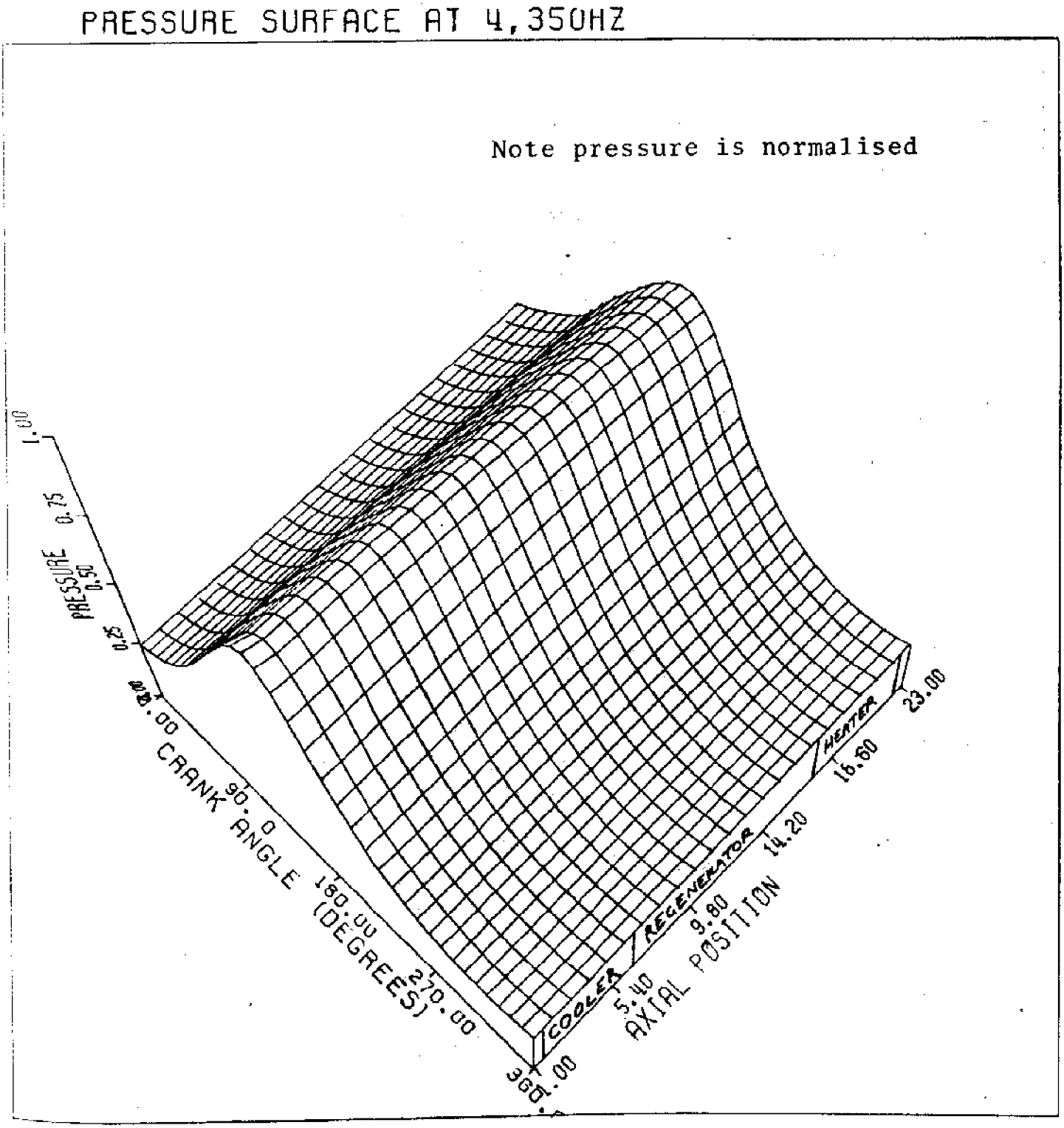


Figure 6.33 Pressure versus Theta and Position in Machine at 4,35 Hz

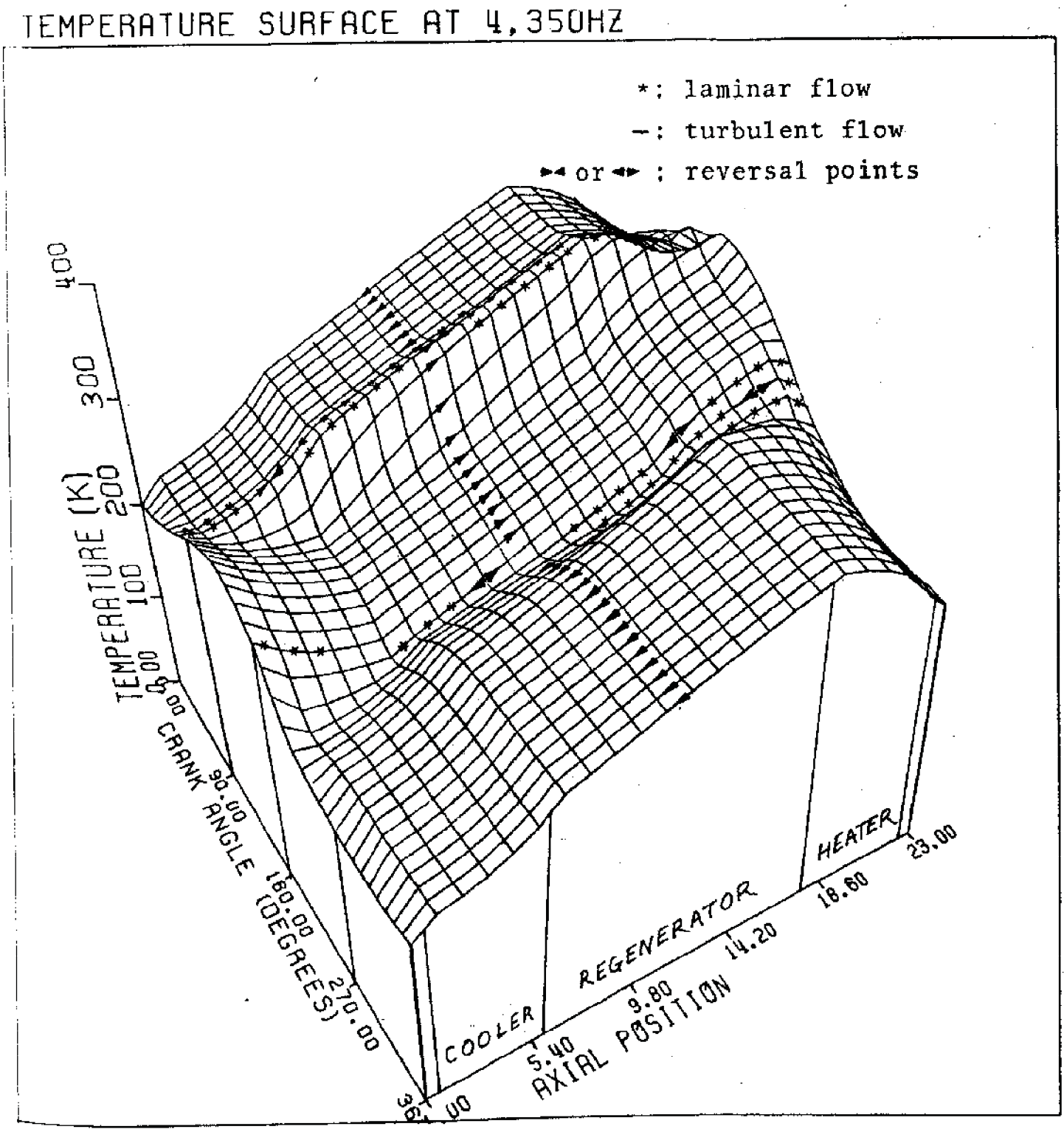


Figure 6.34 Gas Temperature versus Theta and Position in Machine at 4,35 Hz

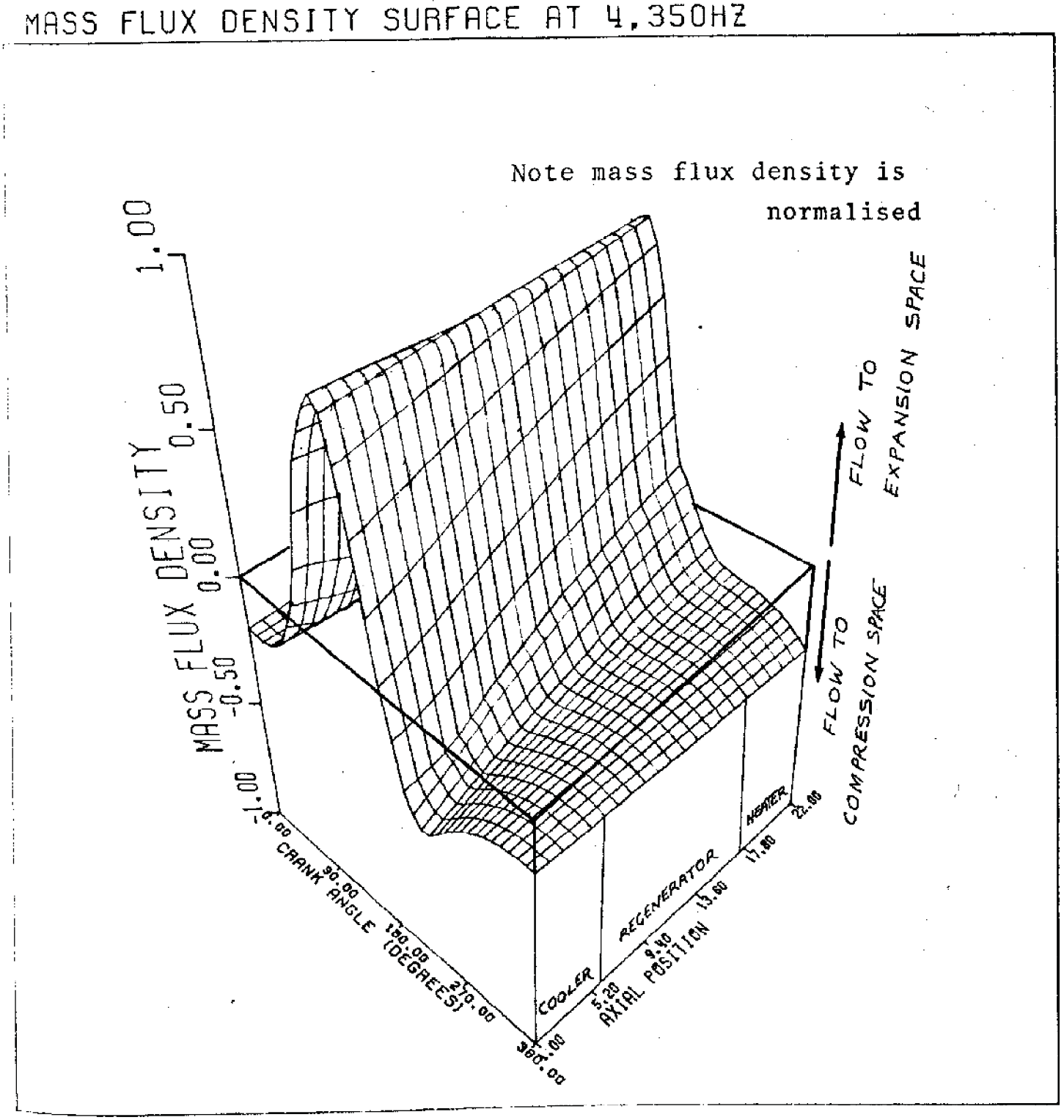


Figure 6.35 Mass Flux Density versus Theta and Position in Machine at 4,35 Hz

7 IDEAL ANALYSES AND SIMULATION RESULTS

Introduction

Both the Schmidt and the second order ideal pseudo-Stirling analyses are evaluated for the 4,35 Hz case only.

The following simulation and ideal analyses are presented:

1) pressure profiles (Schmidt and pseudo-Stirling, Figures 7.1 and 7.2 respectively)
2) work rate and cyclic work (Schmidt and pseudo-Stirling, Figures 7.3 and 7.4)
3) heat rates and the cyclic heat transferred in the cooler, heater and regenerator (Schmidt, Figures 7.5 and 7.6 and pseudo-Stirling, Figures 7.7 and 7.8).
4) working space temperature profiles (pseudo-Stirling only, Figure 7.9).
5) flow reversal points or stagnation planes (Schmidt only, Figure 7.10).

The operation temperatures for the ideal analyses have been calculated as follows: For the Schmidt analysis the two isothermal temperatures are taken as the average cooler and heater gas temperatures averaged again with the respective working space gas temperature.

For the ideal pseudo-Stirling analysis the isothermal cooler and heater temperatures are taken respectively as the average cooler and heater gas temperatures. All these average temperatures were calculated from the simulation results. This procedure was found to give the best correlation between the ideal analyses and the computer simulation.

PLOT ERROR ±0.02BAR

FREQUENCY 4.350HZ

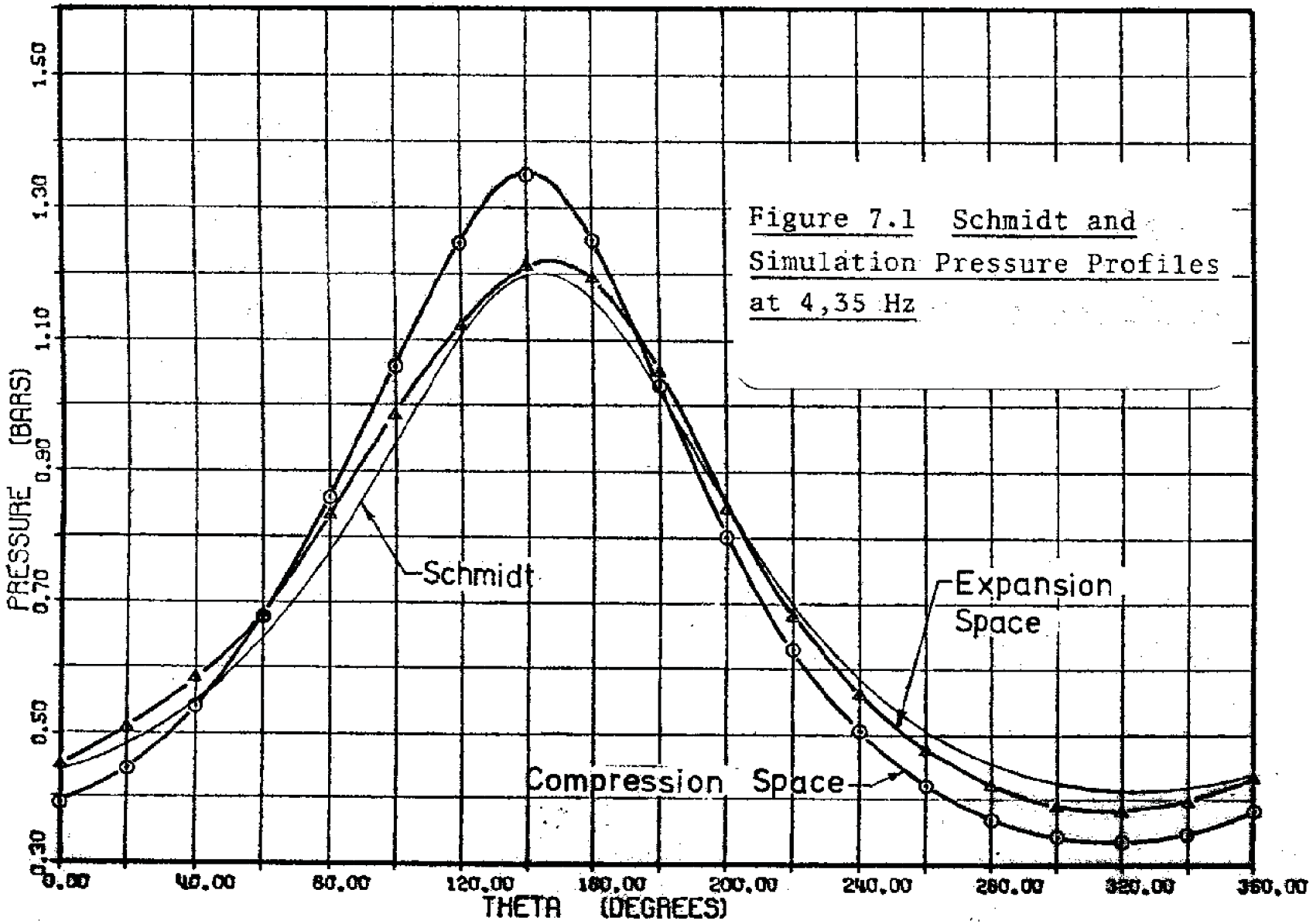


Figure 7.1 Schmidt and Simulation Pressure Profiles at 4,35 Hz

PLOT ERROR ±0,02BAR

FREQUENCY 4,35OHZ

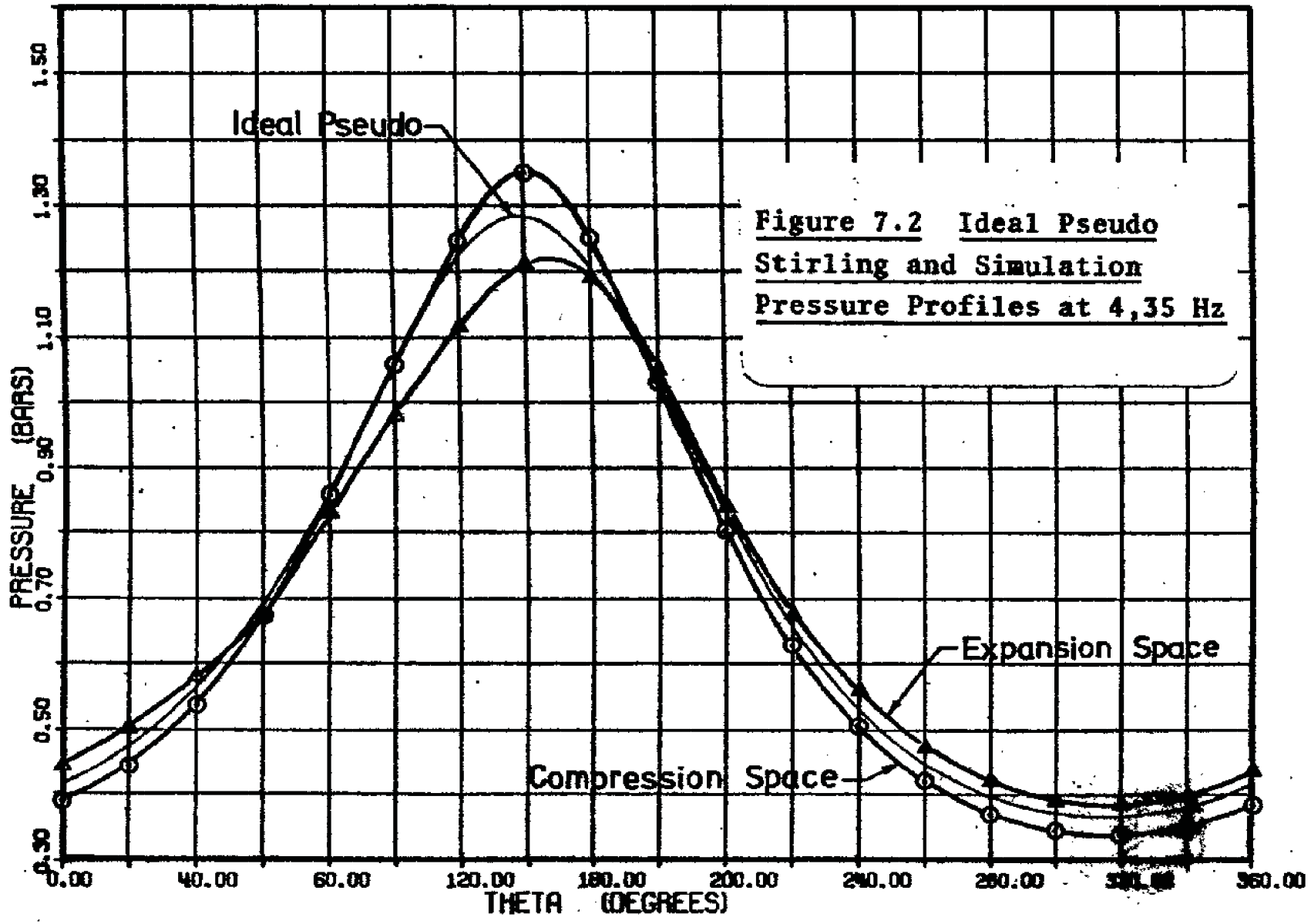


Figure 7.2 Ideal Pseudo Stirling and Simulation Pressure Profiles at 4,35 Hz

PLOT ERROR ±5.0WATTS
CYCLIC WORK 6.400 J

FREQUENCY 4.350 HZ

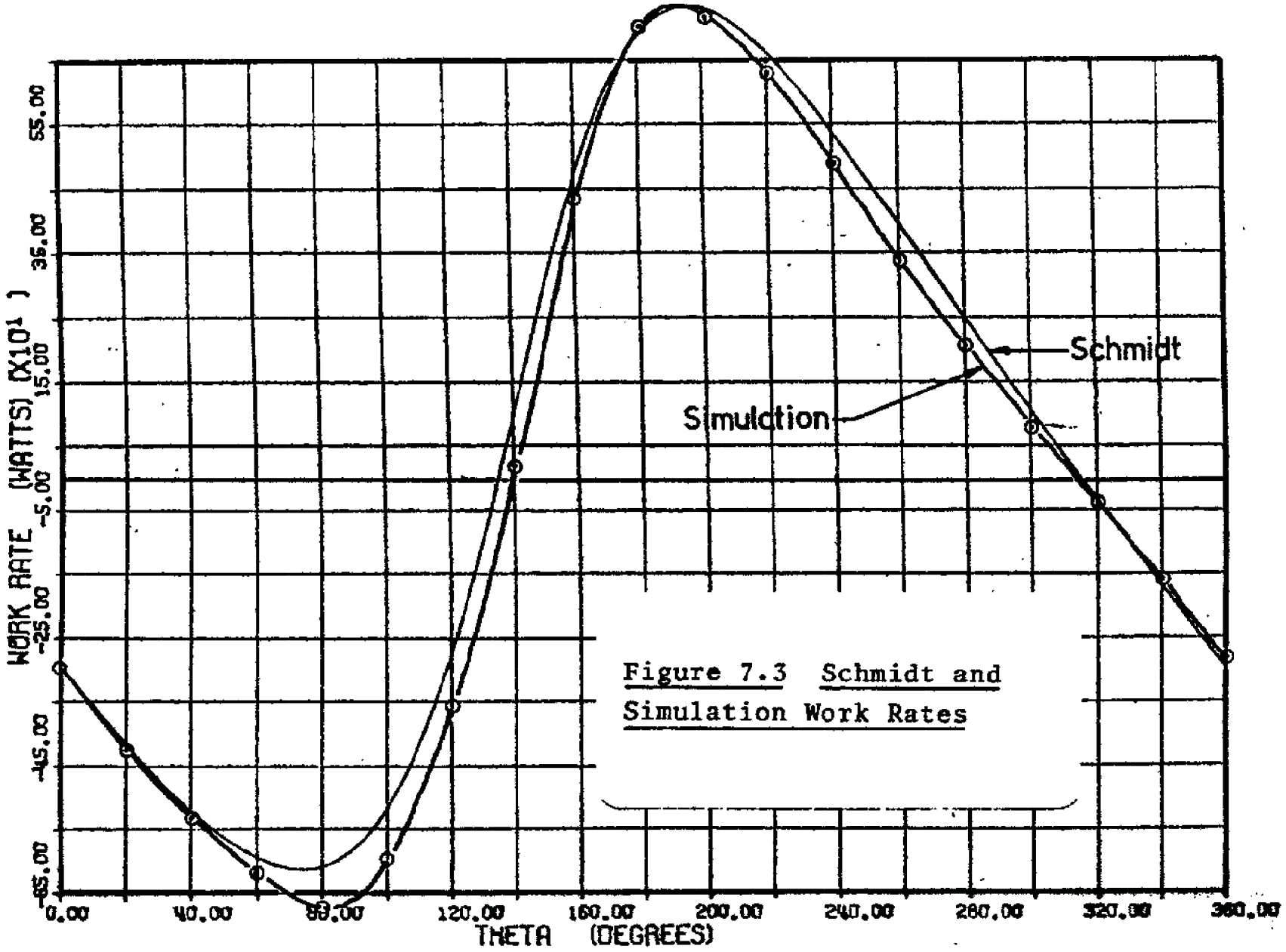


Figure 7.3 Schmidt and Simulation Work Rates

PLOT ERROR ±5,0WATTS

FREQUENCY 4.350HZ

COOLER ⊙ CYCLIC COOLING -16.624 J

HEATER ▲

CYCLIC HEATING 23.024 J

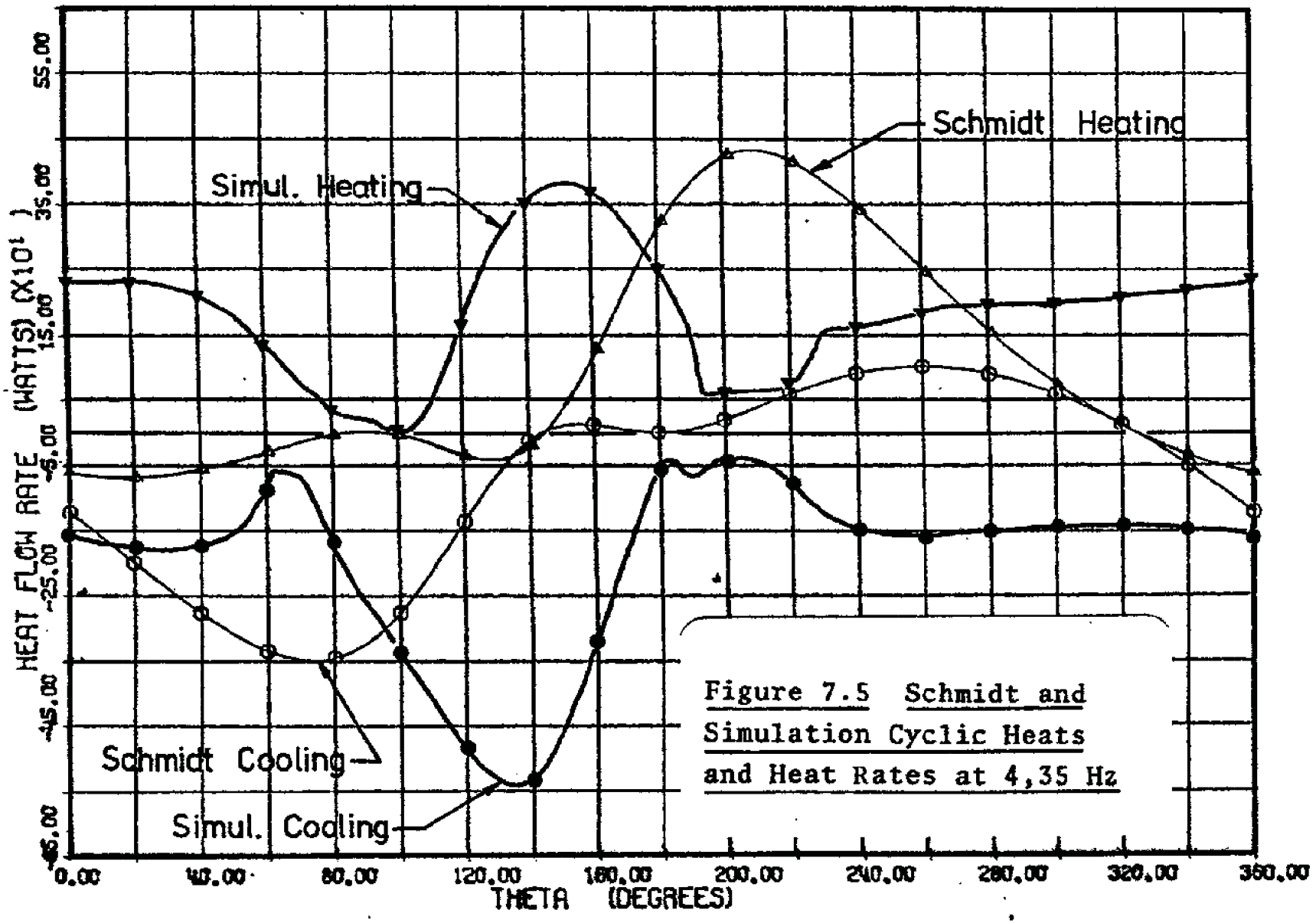


Figure 7.5 Schmidt and Simulation Cyclic Heats and Heat Rates at 4,35 Hz

FREQUENCY 4.350HZ

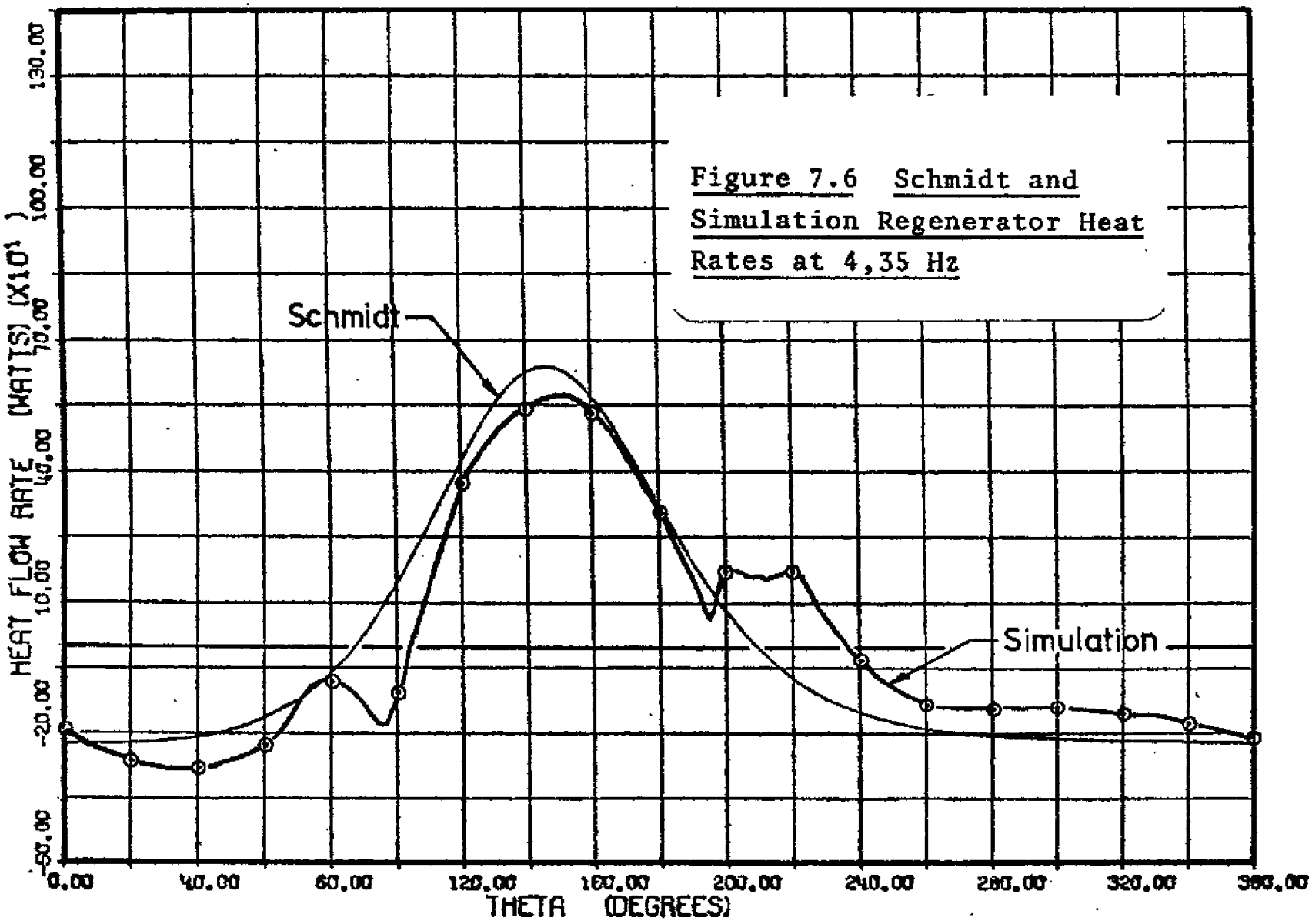


Figure 7.6 Schmidt and Simulation Regenerator Heat Rates at 4,35 Hz

FREQUENCY 4.350HZ

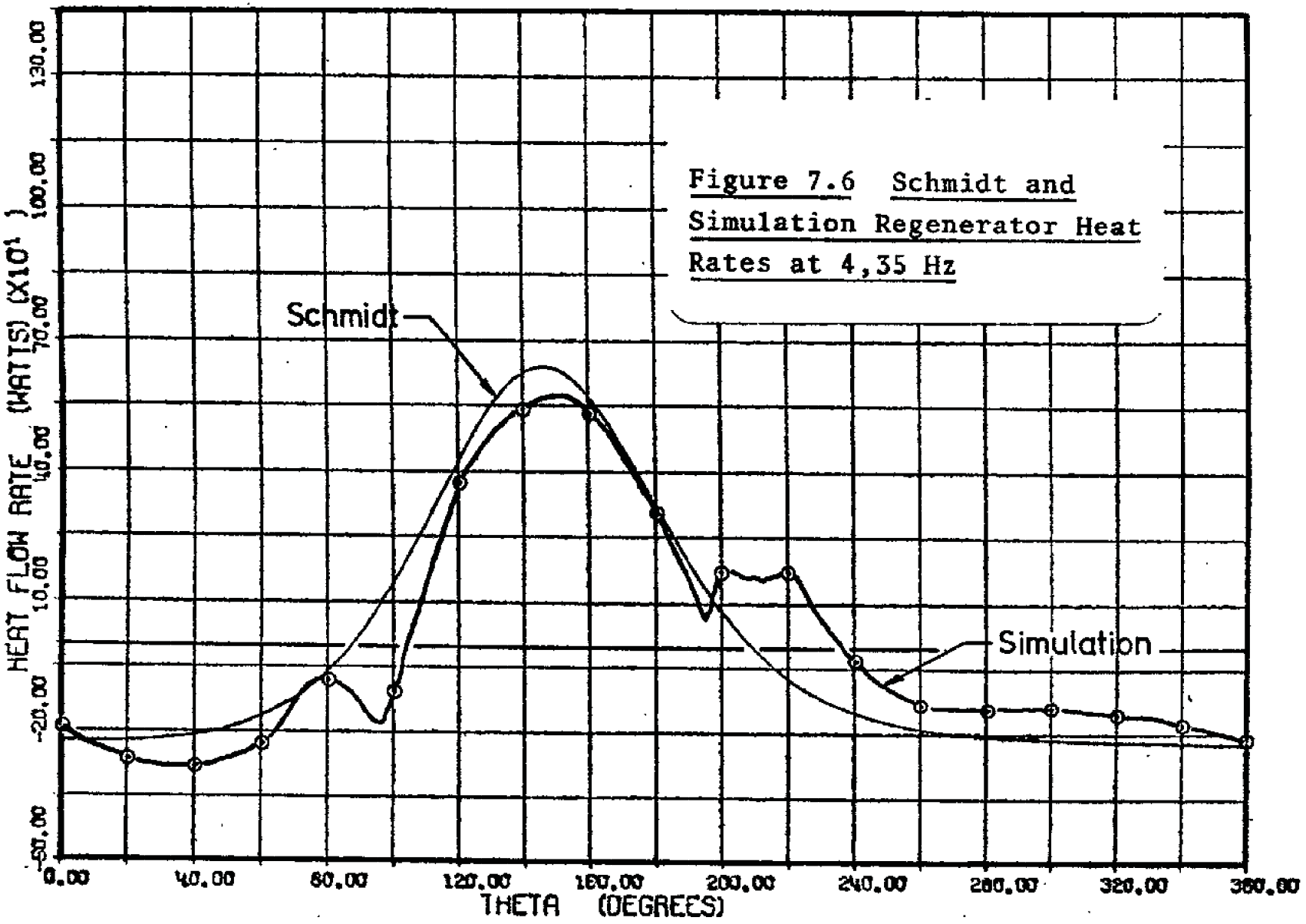


Figure 7.6 Schmidt and Simulation Regenerator Heat Rates at 4,35 Hz

PLOT ERROR ±5.0WATTS

FREQUENCY 4.350HZ

COOLER ⓘ CYCLIC COOLING -23.871 J

HEATER ⚠

CYCLIC HEATING 25.681 J

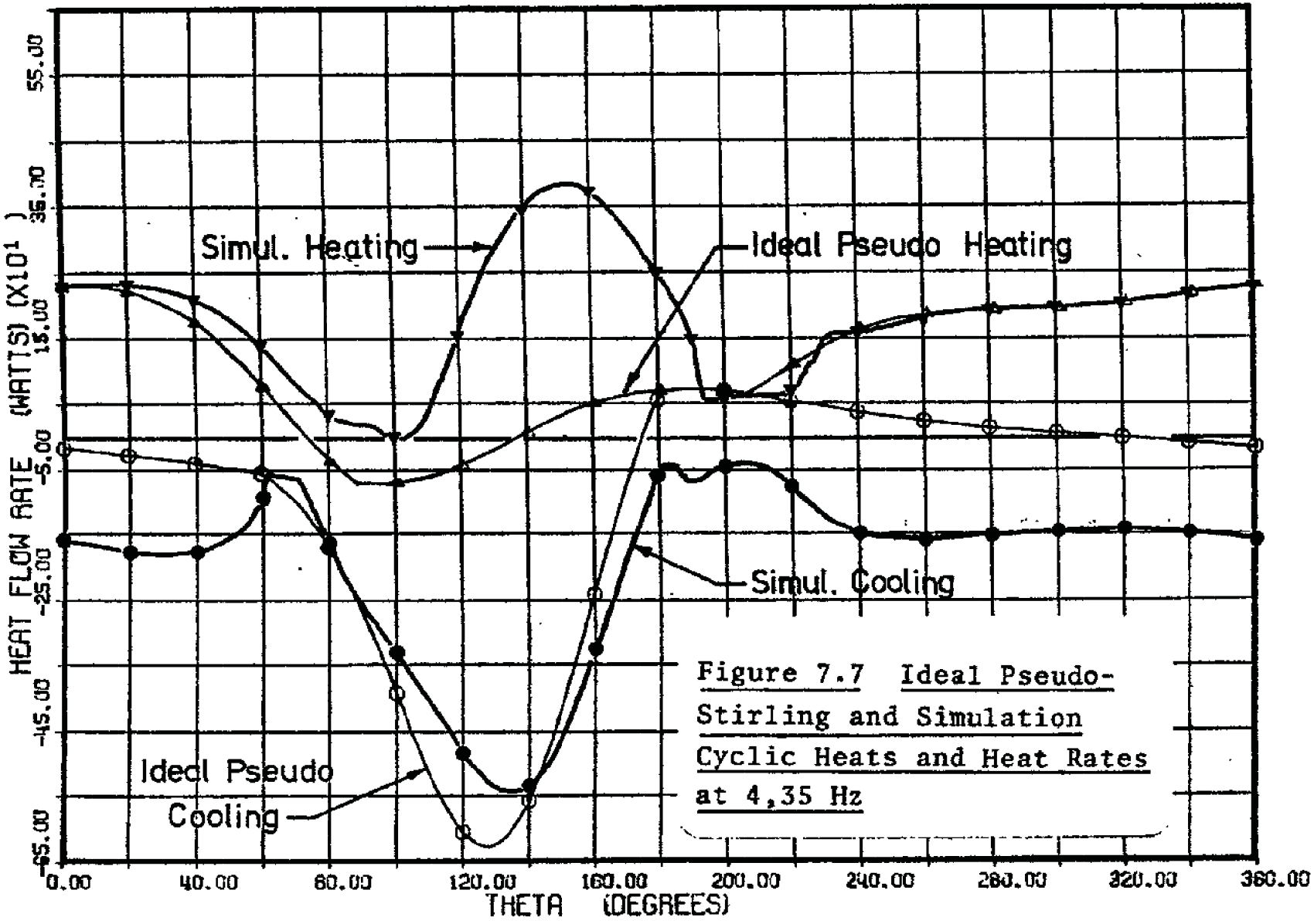


Figure 7.7 Ideal Pseudo-Stirling and Simulation Cyclic Heats and Heat Rates at 4,35 Hz

PLOT ERROR ±5.0WATTS

FREQUENCY 4.350HZ

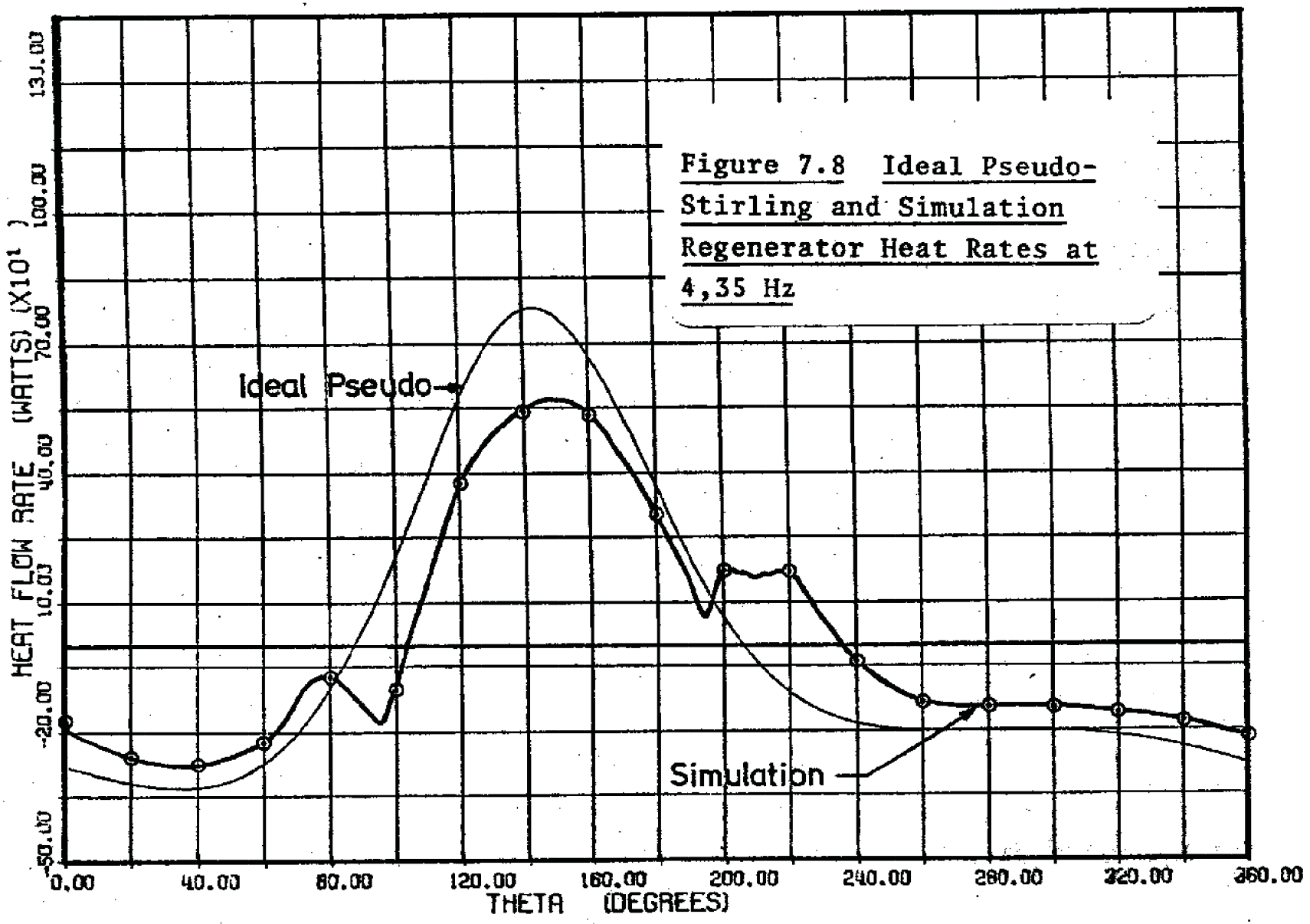


Figure 7.8 Ideal Pseudo-Stirling and Simulation Regenerator Heat Rates at 4,35 Hz

PLOT ERROR ±0,5K

COMPRESSION SPACE ○
EXPANSION SPACE △

FREQUENCY 4.350HZ

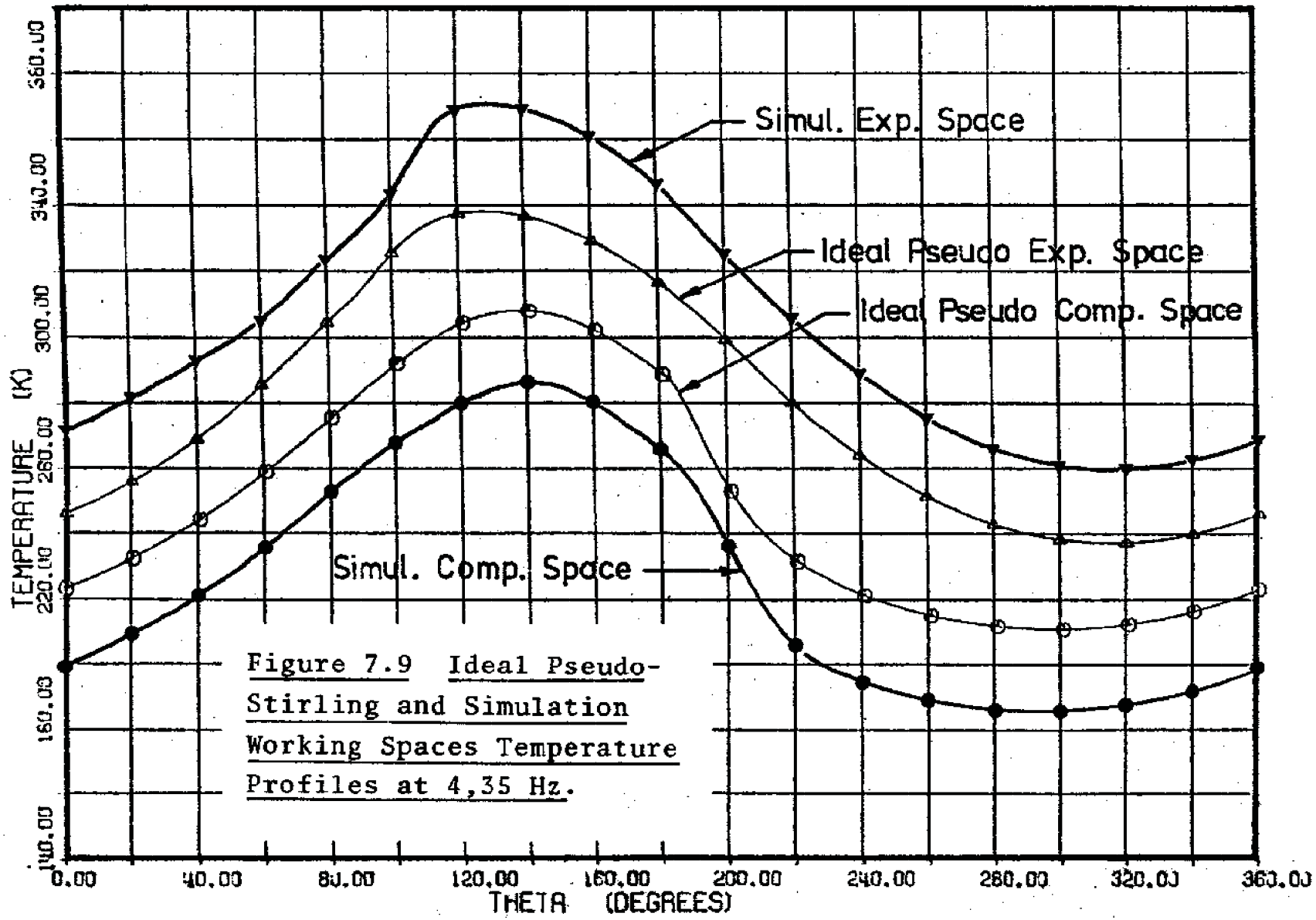
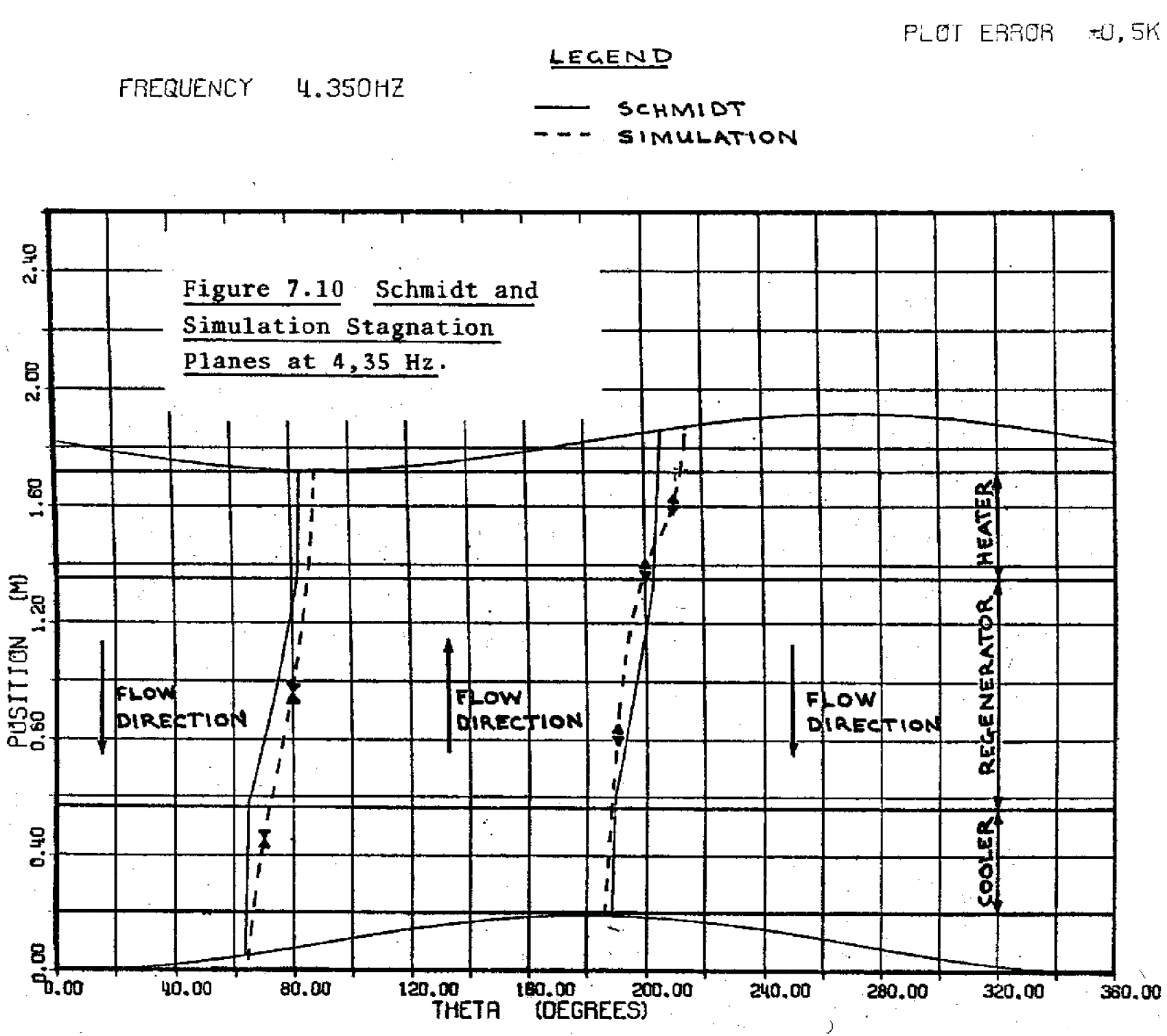


Figure 7.9 Ideal Pseudo-Stirling and Simulation Working Spaces Temperature Profiles at 4,35 Hz.


PLOT ERROR ±0,5K
LEGEND
SCHMIDT
SIMULATION
FREQUENCY 4.350HZ
Figure 7.10 Schmidt and Simulation Stagnation Planes at 4,35 Hz.
POSITION (M)
2.40
2.00
1.60
1.20
0.60
0.40
0.00
FLOW DIRECTION
FLOW DIRECTION
FLOW DIRECTION
HEATER
REGENERATOR
COOLER
0.00
40.00
80.00
120.00
160.00
200.00
240.00
280.00
320.00
360.00
THETA (DEGREES)

8 DISCUSSION OF THE RESULTS

8.1 Introduction

It is important to use as many cells as possible to obtain the full accuracy of the simulation technique. In this work, the number of cells was limited by the available computer budget. For the same reason, convergence was assumed once the regenerator residual heat had dropped to less than 0,25% of the heat supplied at the heater.

All the results are discussed qualitatively, ie, no correlation functions or coefficients are presented.

8.2 Experimental and Simulation Results

The compression space pressure profiles (Figures 6.4 to 6.6) were found to show increasingly better agreement with speed. Overall correlation is good.

The expansion space pressure profiles (Figures 6.7 to 6.9) do not correlate as well as those for the compression space. In the former there is no obvious effect of speed on the degree of correlation. The amplitudes, however, are similar which indicates that the pressure drop across the system as calculated by the simulation is reasonable. There is a tendency for the upper portions of the expansion experimental and simulation profiles to be out of phase with each other. The lower portions show better agreement.

The phase displacements of the simulation pressure profiles can be checked with the result derived from acoustic theory in Appendix C. Based on the average gas temperatures in the cooler

and heater, the following phase angles are calculated:

2,50 Hz : $3,2^{o}$
3,35 Hz : $5,6^{o}$ (acoustic theory)
4,35 Hz : $7,3^{o}$

From Figures 6.1 to 6.3 by inspection, the approximate phase displacements of the simulation pressure profiles at their peaks are:

2,50 Hz : 3^{o}
3,35 Hz : 5^{o} (simulation)
4,35 Hz : 7^{o}

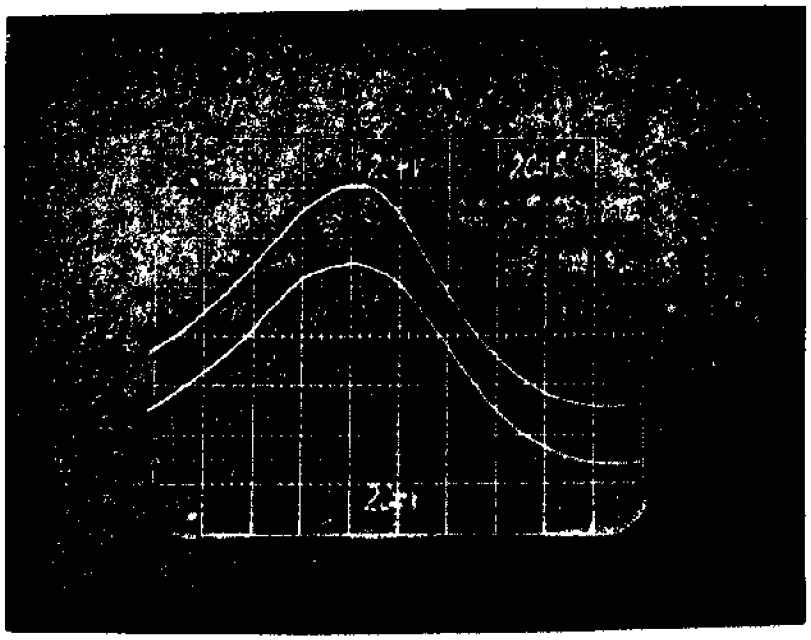
The acoustic theory derivation of the phase displacement only applies from the beginning of the cooler to the end of the heater. The working spaces have thus been assumed to make negligible contribution to the phase displacement.

For the simulation the momentum equation is directly responsible for the phase displacement between the pressure profiles. However, since momentum effects have been ignored in the working spaces, the phase displacement as predicted by the simulation is also only valid from the beginning of the cooler to the end of the heater.

Therefore, the agreement between the acoustic theory and the simulation indicates that the gas momentum has been effectively accounted for over the cooler, regenerator and heater.

The highest expected error associated with the reconstructed experimental pressure profiles is approximately $\pm$ 1% (Appendix O). This error is strongly apparent at the points of smallest change, ie, the peaks and troughs of the profile. It is thus

not possible to determine the phase displacement at their peaks with any certainty. Since the oscilloscope allows both pressure traces to be concurrently recorded, it was decided to check the phase relationship between the experimental profiles directly from the oscilloscope (Figure 8.1).



Note that the profiles have been displaced vertically from each other by one major division.

Figure 8.1 Phase Relationship of the Experimental Pressure Profiles

From Figure 8.1 it appears that the expansion space pressure profile leads in the upper portion of the profiles. However, in the middle and lower sections, the compression space profile appears to be leading. This distortion of the pressure profiles has not been accurately accounted for by the simulation.

Since it has been argued that the gas momentum has been effectively accounted for over the cooler, regenerator and heater, it appears thus that the disagreement between the experimental and simulation results can only be due to gas momentum effects in the working spaces. It is therefore likely that the assumption of negligible mass flux density (and consequently negligible gas momentum) in the working spaces is a source of error.

The wall temperature distribution (Figures 6.10 to 6.12) also tends to indicate increasingly better correlation with speed. It is important to note, however, that the temperatures were measured on the outside of the copper tubes, whereas the simulation calculates the mean bulk temperature of the copper tubes at any station. It would therefore be expected that the experimental and simulation distributions should be slightly different.

The indicated work rate profiles (Figures 6.13 to 6.15) show excellent agreement for all the tests. However the indicated cyclic work does not correlate well. This quantity was very small for each test and it is likely that the simulation results are swamped by truncation errors. Table 8.2 shows that the error in the overall energy balance is approximately of the same order as the indicated work for the 3,35 Hz and 4,35 Hz tests.

Table 8.1 presents the experimental and simulated cyclic heats transferred at the cooler and heater.

TABLE 8.1 EXPERIMENTAL AND SIMULATION CYCLIC HEATS

	COOLER [J]			HEATER [J]		
Speed [Hz]	Simul.	Exprmnt.	% Diff.	Simul.	Exprmnt.	% Diff.
2,50	-46,628	-53,655	-13,1	49,047	56,516	-13,2
3,35	-46,384	-53,895	-13,9	46,219	51,387	-10,1
4,35	-44,690	-51,227	-12,8	42,288	41,156	+ 2,8

The highest expected error associated with the experimental heats is $\pm$ 2,4% at 2,50 Hz and $\pm$ 0,6% at 4,35 Hz for cooling and $\pm$ 7% at 2,50 Hz and $\pm$ 3% at 4,35 Hz for heating (Appendix O). It thus appears that the simulation consistently underpredicts the heat transfer in the cooler and heater in five tests out of six. The cyclic heat input at 4,35 Hz is the only inconsistency which may be attributable to some extraneous experimental error.

The truncation errors associated with the simulation results have not been determined. It is therefore not possible to quantitatively indicate how well the simulation predicts the cyclic heats. Besides this, there are three major factors which could influence these results:

1) The adiabatic working space assumption. In general the respective working space cylinder wall would be at a lower temperature than the gas in the hot end, and at a higher temperature than the gas in the cold end. Consequently the heater will transfer more heat to, and the cooler will extract more heat from the working gas. This is in agreement with the overall trend of the experimental heat transfer results.

2) The use of the Reynolds' analogy based on quasi-steady friction factors. It is probable that the flow profiles and boundary layers are partially disrupted in flow reversal conditions. This could induce greater heat transfer and better mixing of the flow which may in turn cause the Reynolds' analogy to underpredict the local heat transfer coefficients. However, in view of the closeness of the experimental and simulation results, it would appear that the Reynolds' analogy has worked well.

3) The steady flow definition of the laminar/turbulent transition point. In the real situation, the laminar region is likely to be much smaller than that predicted by the simulation. At 4,35 Hz the simulation indicates that the laminar region is limited to 9,6% of the entire flow cycle. At 2,50 Hz the laminar region rises to 17,6%, nearly twice that for 4,35 Hz. This, coupled with the integral technique's inherent inaccuracy in modelling laminar flow, could introduce some error. This point can be noticed in the comparisons between the experimental and simulation pressure profiles and temperature distributions. However, the cyclic heats do not directly indicate any effect of machine speed on the degree of correlation.

An attempt was made to measure the average gas temperatures in the working spaces (Figures 6.22 to 6.24). The correlations here are poor. Since all the other experimental correlations are good, it would appear that there is a systematic error involved. The thermocouples used were not shielded from radiation and were located very close to the cylinder heads. Consequently they could have suffered radiation and conduction errors. It is therefore felt that these experimental temperatures are not an accurate indication of the mean gas temperatures in the working spaces.

Simulation results for 4,35 Hz only using the central difference momentum algorithm are presented in Figures 6.25 to 6.33. Comparing these results with the respective 'upstream' results a slightly weaker overall agreement is indicated between the 'central difference' results and experiment. This is especially evident in the pressure profiles, temperature distribution and the indicated cyclic work. The indicated cyclic work however, may still be within truncation error limits. Even though slightly better correlation is apparent by using the upstream difference, a full investigation is not possible on one run. What is indicated is that the central difference technique is stable and well behaved and gives reasonable results. This observation is contrary to the belief that an upstream difference is a necessity for stability.

Table 8.2 presents the overall energy balance for both the simulation and experimental runs. The energy balance error is defined as follows:

$$\varepsilon_b = (Qk + Qh - W)/Qh \qquad (8.1)$$

The energy balance errors are small for the simulation in general. Ideally these errors should be the result of truncation and round-off errors only. The 'central difference' run

indicates a higher energy balance error than for the 'upstream' runs. This could be due to lack of convergence, since no effort was made to converge this run to the same degree as the other runs.

TABLE 8.2 OVERALL ENERGY BALANCES

	Speed [Hz]	Qk [J]	Qh [J]	W [J]	Energy Balance error	Efficiency
Simulation	2,50	-46,628	49,047	2,886	-0,95%	5,88%
	3,35	-46,384	46,219	1,261	-3,09%	2,73%
	4,35	-44,690	42,288	-1,172	-2,91%	-2,77%
	4,35*	-44,655	42,605	-0,287	-4,14%	-0,67%
	*(Central Diff.)					
Exprmnt.	2,50	-53,655	56,516	4,127	-2,24%	7,30%
	3,35	-53,895	51,387	2,592	-9,92%	5,04%
	4,35	-51,227	41,156	-0,860	-22,38%	-2,09%

The energy balance errors for the experimental results are larger than for the simulation. This is most likely due to the energy transferred in the working spaces which was not accounted for.

8.3 Ideal Analyses and Simulation Results

The comparison between the ideal analyses and the simulation (Figures 7.1 to 7.11) is presented for 4,35 Hz only. In general there is an overall better agreement for the ideal pseudo-Stirling analysis than for the Schmidt analysis. This is simply due to the fact that the ideal pseudo-Stirling analysis approximates the simulated configuration more closely. However, it is still important to know how well the Schmidt analysis can predict such systems.

The Schmidt pressure profile (Figure 7.1) has approximately the same amplitude as the simulation expansion space profile. This observation was also made by Walker [Wa73] where, in addition, he indicated that the phasing was that of the compression space profile. In this work the phasing appears to be more in line with the expansion space. The actual peak occurs between that of the expansion and compression pressure profiles.

The ideal pseudo-Stirling pressure profile (Figure 7.2) is located approximately at the average of the two simulation profiles. The phasing tends to coincide with the compression space profile.

The indicated work rate profiles (Figures 7.3 and 7.4) are both similar to the simulation profile. Both analyses obviously overpredict the indicated cyclic work, the ideal pseudo-Stirling less so than the Schmidt. The efficiencies predicted by the Schmidt and ideal pseudo-Stirling analyses are 28% and 7% respectively, as against the simulations prediction of -2,77%.

The ideal heat rate profiles and the cyclic heats transferred at the cooler and heater are presented in Figures 7.5 and 7.7. Here it can be seen that the heat rate profiles as predicted by the Schmidt analysis are completely dissimilar to those generated by the simulation. The ideal pseudo-Stirling, on the other hand, does predict similar heat rate profiles. It is interesting to note that both ideal analyses indicate that there are certain stages in the cycle in which heat is in fact rejected to the hot heat exchanger and added from the cold heat exchanger. This situation is more prevalent in the Schmidt analysis, and raises important considerations when designing pure Stirling machines. In general the heat exchangers

would have to be designed to supply the maximum heat rates. This can conveniently be achieved by including local thermal buffer stores. This would allow constant heat fluxes between the heating source and the cooling sink and the respective thermal store. Also the opposing heat requirements at the heat exchangers would be satisfied.

The heat rate profiles for the regenerator (Figures 7.6 and 7.8) show similar agreement with slightly better correlation for the Schmidt analysis. The discontinuities that are evident in the simulation profile occur during reversal and relaminarisation of the flow. These discontinuities can also be noticed to a lesser extent in the heat rate profiles of the cooler and heater. The ideal and simulation profiles show the correct relationship to each other, in that the ideal analyses predict a greater exchange of heat with the regenerator.

The working space gas temperature profiles as calculated by the ideal pseudo-Stirling analysis (Figure 7.9) are similar but displaced from their respective simulation profiles. The ideal expansion space temperature profile is lower than the respective simulation temperature profile and *vice versa* for the compression space. In the case of the simulation the gas enters the expansion space at a higher temperature than for the ideal analysis and *vice versa* for the compression space. These results are therefore consistent with what would be expected.

The flow reversal planes as predicted by the Schmidt analysis (Figure 7.10) show reasonable agreement with the simulation. This would appear to indicate that the mass flows as predicted by the Schmidt analysis are reasonable. In turn, this implies that the main mechanism of working gas transport is by displacement, since the Schmidt analysis assumes no pressure drop across the system.

9 CONCLUSIONS, DEVELOPMENTS AND RECOMMENDATIONS

9.1 Conclusions

The following points are evident from the analytical and experimental work presented in this study:

1) The simulation approach first presented by Urieli has the potential for predicting the thermodynamic behaviour of a particular machine with an acceptable degree of accuracy.

2) Urieli's analysis has certain discrepancies (Section 3.2).

3) These discrepancies can be resolved by a more rigorous approach to the derivation of the transport equations (Appendix D).

4) The simulation results of this study are consistent in so far as no major contradictions are evident when compared to experimental and ideal results (Chapters 6 and 7).

5) The assumption of negligible gas momentum in the working spaces is in error (Section 8.2).

6) The definition of the laminar, turbulent and transition regimes is in error. This error appears to decrease with increased speed (Section 8.2).

7) The assumption that the working spaces are perfectly adiabatic is obviously a source of error (Section 8.2). However, for the machine investigated, this was not too significant.

8) The irrecoverable pressure drop as defined for steady flow systems is unsuitable for non-steady flow systems. In redefining the irrecoverable pressure drop in terms of eddy dissipation, better results were obtained (Appendix E).

9) The instantaneous pressure drop can be successfully evaluated using steady flow friction factor data.

10) The imperfect heat transfer can be successfully evaluated using Reynolds' analogy.

11) An increase in the accuracy of modelling the viscous resistance and viscous dissipation can be obtained by the inclusion of the normal stress terms (Appendix E).

12) The upstream differencing for the momentum equation is not necessary for stability - central differencing gives perfectly stable results (Section 8.2).

13) The phase displacement between the compression and the expansion space pressure profiles can be accurately calculated using simple accoustic theory (Appendix C).

14) The Schmidt theory is not the ideal yardstick for Stirling machines in which the heat transfer is mainly effected through separate heat exchangers (ie, pseudo-Stirling machines) (Sections 2.2 and 8.3).

15) The ideal maximum efficiency is only equal to Carnot's efficiency for the case in which all net heat transfer occurs at the working spaces (ie, pure Stirling machines) (Sections 2.2 and 2.3).

16) The gas flow distribution in Stirling type machines is mainly a function of displacement (Section 8.3).

9.2 Developments

Contributions to the present state of knowledge in this field are:

1) The derivation of the complete transport equation set in both differential and integral forms (Appendix D). This was done with special reference to Stirling machines. It is noted, however, that all these equations have been previously derived for general applications by other workers.

2) The technique for empirically modelling the viscous dissipation (Appendix E).

3) The derived result for calculating the phase displacement between the pressure profiles of the working spaces (Appendix C).

4) The derived closed form solutions for calculating the position of the flow reversal planes (Appendix A).

5) The solution of the ideal pseudo-Stirling analysis for the case of non-sinusoidal piston motions (Appendix B).

9.3 Recommendations for Future Work

The use of the momentum equation should be extended to account for the momentum of the gas in the working spaces. This would be a simple modification to the present system.

The conditions in oscillating flow for which transition to laminar or turbulent flow occurs should be determined.

Efforts should be directed towards the determination of empirical formulae which can be used to calculate the instantaneous heat transfer coefficients in the working spaces.

Truncation errors in the simulation model can have a significant effect on accuracy. These errors should be investigated.

Finally, it is important that optimisation techniques be developed for the simulation model. Once this has been achieved the potential for practical application, especially in the field of design, can be fully realised.

APPENDIX A

THE IDEAL SECOND ORDER STIRLING CYCLE (SCHMIDT)

All parameters in this section are dimensional.

A.1 Introduction

The Schmidt analysis is one step removed from the ideal first order Stirling cycle analysis [RU77] in that the gas is recognised as being in differing thermodynamic states throughout the machine. No losses are allowed for and it is thus possible to obtain a closed form solution for the general case. G. Schmidt first obtained this solution - or a similar form of it - in 1871 [Sc1871].

In addition to the above, it is shown here that it is possible to evaluate the ideal instantaneous heat fluxes and the instantaneous mass velocities within the system.

It is generally assumed in this type of analysis that each element of the working gas is at all times in thermal equilibrium with the walls immediately adjacent to it. This implies perfect heat transfer with no wall-to-gas temperature differences. The predicted energy requirements are in consequence extremely optimistic [Wa73]. If, however, it is possible to determine the average gas temperatures in the heat exchangers by some other means, then using these gas temperatures in the analysis would lead to a better prediction of the energy requirements (this is indicated in Chapter 7).

The basic horizontally opposed (alpha) arrangement is assumed in this analysis - this is not a limitation since most Stirling